Int. J. Heat Mass Transfer. Vol. 29, No. 1, pp. 69–82, 1986
Printed in Great Britain

0017–9310/86 $3.00 + 0.00

An experimental investigation of mixed cavity natural convection in the high Rayleigh number regime

A. T. KIRKPATRICK* and M. BOHN†

* Department of Mechanical Engineering, Colorado State University, Fort Collins, CO 80523, U.S.A.
† Solar Energy Research Institute, Golden, CO 80401, U.S.A.

(*Received* 2 *January* 1985 *and in final form* 22 *July* 1985)

Abstract—Using four different configurations of differentially heated and cooled vertical and horizontal surfaces in a cubical enclosure, natural convection experiments at high Rayleigh numbers were conducted. All of the experiments were variations of the heating-from-below case. Experimental measurements and observations were made of the heat transfer, flow patterns, and the mean and fluctuating temperature distribution. The results indicated that the heated floor promoted mixing in the enclosure and reduced the thermal stratification. For the boundary conditions of the experiment, the heat transfer from the horizontal surfaces was not strongly affected by the presence of a horizontal temperature gradient.

1. INTRODUCTION

MIXED cavity natural convection results from the heating or cooling of an enclosure in both the horizontal and the vertical directions. A great deal of research has been performed on the two limiting cases of vertical enclosures heated from below and cooled from above, and horizontal enclosures differentially heated from the side. However, the more general mixed cavity case has not been extensively studied. This problem has applications in the thermal engineering of buildings, nuclear reactors and solar collectors, and in other natural convection problems where the heat transfer between vertical surfaces can be of the same order as heat transfer between horizontal surfaces. In a mixed cavity at high horizontal and vertical Rayleigh numbers, thermals rise and fall in the vertical direction and interact with boundary layers moving along the inside perimeter of the cavity.

Mixed cavity natural convection has been investigated numerically for laminar flow by Chan and Banerjee [1] and Shiralkar and Tien [2]. A review of the experimental and analytical work on the effect of vertical side walls on heating from below is given by Catton [3]. The related stabilizing case of heating from above and from the side has been experimentally studied in the laminar regime by Ostrach and Raghavan [4], and numerically by Berkovsky *et al.* [5].

The turbulent regime (vertical Rayleigh numbers Ra_h above 10^6) of the first limiting case of heating from below and cooling from above has been investigated by Somerscales and Gazda [6], Chu and Goldstein [7] and Garon and Goldstein [8], among others. The experimental observations indicate that the heat transfer between the bottom and top surfaces is achieved by cyclic generation and release of thermals. The mean temperature gradient in the vertical direction can have a reversal due to buoyant thermals moving from one surface to the opposite surface without dissipating in the core. Hollands *et al.* [9] have developed a steady conduction-layer analysis to model the heat transfer. Their analysis requires an empirical constant that is dependent on the Prandtl number. The empirical constant can be determined from experiments on upward-facing single plates in an extensive fluid. Using data for water given by Fujii and Imura [10], the steady conduction-layer model predicts that

$$Nu_h = 0.103 Ra_h^{1/3}. \tag{1}$$

The 1/3 power law is an asymptotic limit for large Rayleigh numbers since Rayleigh number exponents between 0.278 and 0.305 have been reported for water. Howard [11] has developed a cyclic conduction-layer model for the frequency of the thermals which has been experimentally confirmed by Sparrow *et al.* [12].

The second limiting case of the mixed cavity is an enclosure differentially heated from the side. For this configuration the flow structure at horizontal Rayleigh numbers, Ra_l, above 10^4 is a laminar boundary layer parallel to the walls. The heat transfer mechanism is convection in boundary layers along the enclosure surfaces. The core region is relatively inactive and nearly isothermal in the horizontal direction and it has a near linear temperature gradient in the vertical direction. Experimental data and correlation equations for water at Rayleigh numbers greater than 10^8, aspect ratios at or near 1, and adiabatic top and bottom surfaces have been given in MacGregor and Emery [13] and, more recently, in Bohn *et al.* [14]. At Rayleigh numbers of the order of 10^{10}, the beginning of the transition to turbulent boundary-layer flow has been observed. Raithby *et al.* [15] have applied a laminar conduction-layer model to this configuration and predict that

$$Nu_l = 0.670 Ra_l^{0.25} (h/l)^{-0.25} \tag{2}$$

NOMENCLATURE

A_w	wall surface area [m^2]
g	acceleration of gravity [$m\,s^{-2}$]
h	enclosure height [m]
$\bar{h}$	average heat transfer coefficient [$W\,m^{-2}\,°C^{-1}$]
l	enclosure length [m]
L	characteristic length [m]
Nu	Average Nusselt number, $Q/[A_w(T_w - T_b)]$
Pr	Prandtl number
Q	wall convective heat transfer [W]
Ra	Rayleigh number, $g\beta\Delta TL^3Pr/v^2$
Ra^*	modified Rayleigh number, $Nu \times Ra$
Ra_h	vertical Rayleigh number based on enclosure height h, $g\beta\Delta T_h h^3/v\alpha$
Ra_l	horizontal Rayleigh number based on enclosure length l, $g\beta\Delta T_l l^3/v\alpha$
T_b	bulk temperature; average of the heated and cooled wall temperatures [°C]
T_w	wall temperature [°C]
z	vertical distance from enclosure floor [m].

Greek symbols

β	coefficient of thermal expansion [K^{-1}]
ΔT	temperature difference between the hot and the cold surfaces [°C]
v	kinematic viscosity [$m^2\,s^{-1}$]
σ	standard deviation of temperature fluctuation [°C].

where the Nusselt number is calculated on a wall-to-bulk-temperature difference. This model is strictly valid for aspect ratios greater than 5; however, it is a very good predictor at an aspect ratio of 1, as noted by Bohn *et al.* [14].

For Rayleigh numbers at or above 10^{10}, correlations are not available to predict heat transfer in a situation with simultaneous heating from the side and from below in an enclosure. For the problem of heat transfer in buildings, it is not possible to predict with confidence the rates of heat transfer from the warmer portions of the building to cooler portions, to determine resulting air flow patterns, or to determine resulting air temperatures.

In this paper we examine experimentally the case of high ($\sim 10^{10}$) Rayleigh number natural convection in a water-filled cubical enclosure heated simultaneously from below and from the side. Experimental measurements and observations are made of the heat transfer, the flow patterns and the mean and fluctuating temperature distribution.

2. DESCRIPTION OF EXPERIMENT

Two separate experiments were conducted. The first determined the overall Nusselt–Rayleigh number correlations and the second determined the flow patterns and temperature distributions.

Four configurations were tested, as shown in Fig. 1. All the configurations are variations of the heating-from-below case. The first is the mixed vertical and horizontal configuration with a heated bottom and cooled top with one heated and one cooled side wall, denoted as HHCC. The second is a vertical configuration of heating from below and cooling from above with two cooled side walls, denoted as HCCC. The third configuration is a horizontal configuration of a hot and a cold side wall with a heated bottom and heated top, denoted as HHHC. The fourth is the limiting vertical configuration with heated bottom and cooled top, and conducting side walls, denoted as HC. There are two other possible combinations involving a heated bottom, namely cooled from above and heated from the side, and heated from above and cooled from the side, which were not tested.

The experiments were performed using the test cell shown in Fig. 2. The test cell is the same as described in [14], but turned on its side. It is a cubical enclosure with an interior dimension of 30.5 cm, and is constructed of eight 1.27-cm-thick aluminium plates. It should be noted that the interior length scale was a factor of two larger than previous experiments concerned with heating from below [6–8].

The four inner plates overlap one another and are screwed together with a neoprene gasket to form the enclosure. The four outer plates provide heating and

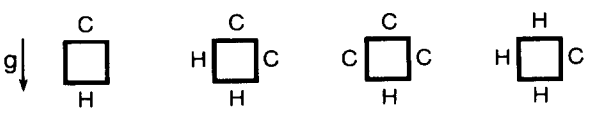

	HC	HHCC	HCCC	HHHC
$Ra_h \times 10^{-10}$ =	0.1-1.45	0.1-1.45	1.45	0
$Ra_l \times 10^{-10}$ =	0	1.45	0	1.45

FIG. 1. Vertical cross sections of the test configurations: HC, HHCC, HCCC and HHHC. Range of vertical and horizontal Rayleigh numbers tested are shown below each figure.

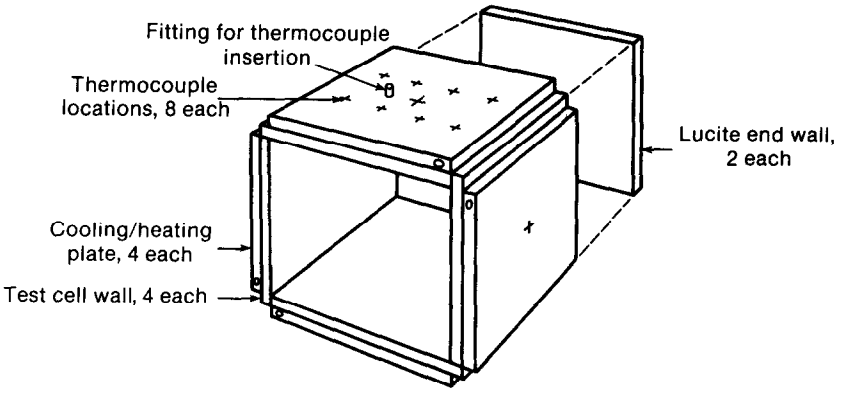

FIG. 2. Schematic of test cell.

cooling to the four enclosure walls via milled channels through which hot or cold water is pumped. The outer plates are sealed and bolted to the inner plates.

The remaining two vertical surfaces are 19-mm lucite plates (for clarity, only one of these lucite end walls is shown in Fig. 2) which allow for flow visualization.

Three of the walls have a centered thermocouple well bored to within 3 mm of the enclosure's inner surface. The top wall has eight such thermocouple wells. These wells are located as shown in Fig. 2. The purpose of these copper–constantan thermocouples is to determine the average wall temperature and spatial variations in the wall temperature across the plate. The spatial variation was less than 10% (typically 5%) of the overall temperature difference $T_h - T_c$. Therefore, the heated and cooled walls can be considered isothermal. For the HC configuration the two vertical aluminum surfaces may be considered perfectly conducting.

The four aluminum test cell walls are insulated with urethane foam board insulation 8.3-cm thick with a thermal resistance of $4.6°C^2\ W^{-1}$. Heat loss from these four walls is estimated to be about 0.1% of the total heat transferred from the walls. The estimate is based on the wall temperature, the outer surface temperature of the insulation and the thermal resistance of the insulation. Loss from the lucite end walls (which were not insulated) is estimated to be about 0.5%. This estimate is based on the highest temperature on the outer surface of the lucite wall, the ambient temperature, and an assumed natural convection heat transfer coefficient of $6\ W\ m^{-2}\ °C^{-1}$. Therefore, the two facing lucite sides may be considered adiabatic. Heat transferred from a hot wall to a cold wall through the neoprene insulation is estimated to be about 0.8%.

A pair of fittings on each outer plate provides water inlets and outlets, and fittings for inserting a thermocouple and an RTD probe in the inlet flow and a second RTD in either the inlet or outlet flow. This arrangement is used to measure the change in the cooling or heating water temperature in the four walls. The RTD probes are placed in opposite arms of a Wheatstone bridge in such a way that the nominal probe resistance, 100 ohms, is cancelled and a bridge output voltage proportional to the temperature difference is produced. The accuracy of the temperature difference measured with this technique is determined by calibration to be $\pm 1\%$ for temperature differences greater than about 0.2°C.

Cooling and heating water flow rates, nominally $500\ kg\ h^{-1}$, are measured with rotameters. These were calibrated by the stopwatch-and-bucket method to within $\pm 0.5\%$ for temperatures near ambient. For the highest temperature the walls were operated, about 65°C, the flow meters tended to read high by about 2–3%, in addition to a decrease of approx. 1.5% in the water density (from 30° to 60°C). Partially offsetting those two errors is an error that increases to about 2% at 65°C due to the nonlinearity of the temperature difference measuring method. Frictional heating in the cooling/heating channels is responsible for about a 1% decrease (increase) in the magnitude of measured heat transfer from (to) the hot (cold) walls. An error analysis based on these four sources of error suggests that the heat transfer measurement for each wall is accurate to $\pm 2\%$. Data are not corrected for conduction through the neoprene gasket from a hot wall to a cold wall (about 0.8%), nor for radiation heat transfer from the hot wall to the cold walls (about 1.6%). Overall heat balances in the test cell (total measured heat transfer from hot walls minus total measured heat transfer to the cold walls divided by measured total heat transfer from the hot walls) are typically better than $\pm 2\%$, although for low-Rayleigh-number tests (less than 0.5×10^{10}), this increases to $\pm 4\%$. An overall wall heat transfer measurement is expected to be within $\pm 5\%$ of the actual convective heat transfer from each surface.

The working fluid in the test cell is deionized water. To eliminate the formation of air bubbles in the test cell, the water is brought to a slow boil for 2 h, allowed to cool, and then poured slowly into the cell. The test cell is carefully leveled with a bubble-type machinist's level. Properties of the water (thermal conductivity, dynamic viscosity, density, coefficient of thermal expansion) in the test cell are calculated at a temperature equal to the

average of the four heated/cooled wall temperatures, which is referred to as the bulk temperature. Specific heat is taken as constant (4.19 J g^{-1} $°C^{-1}$). The length scale used in calculating the Nusselt and Rayleigh numbers is $l = 30.5$ cm, and the area used to derive the heat transfer coefficient is $A_w = 930$ cm^2. The temperature difference used in deriving the Rayleigh number is the difference in temperatures of the hot and cold walls:

$$Ra = \frac{g\beta\Delta TL^3}{\nu^2} Pr.$$

The temperature difference used to calculate the heat transfer coefficient is the difference between the wall temperature and the bulk temperature:

$$Nu = \frac{\bar{h}L}{k}, \qquad \bar{h} = \frac{Q}{A_w|T_w - T_b|}.$$

A shadowgraph is used for flow visualization. The light from a 1-kW quartz lamp is focused by a 38-cm focal length Fresnel lens, passed through a pinhole filter and collimated by a 140-cm focal length Fresnel lens before passing through the two lucite ends of the test cell. Vellum paper is used as the diffuse plane of the shadowgraph. Photographs of the shadow patterns are taken with a 55-mm lens on a 35-mm camera.

Temperature measurements in the enclosure core are made with a copper–constantan thermocouple probe. A rubber septum is installed in a hole drilled through the top plate of the test cell. The L-shaped probe is passed through the rubber septum. The probe can be moved vertically for vertical scans and rotated for horizontal scans. The probe consists of a 0.1-mm wire with a 0.5-mm junction, a glass tube and a metal sleeve. The wire behind the tip is encased in a glass tube drawn to a small point in order to reduce probe conduction. The probe can not be placed closer than 8 mm from the top and bottom surfaces of the test cell, due to the dimensions of the glass and metal sleeve. The thermocouple output is sampled by a HP3497A digital microvoltmeter at a 10 Hz rate for a period of 120 s. The time constant of the probe is calculated to be 0.1 s, an order of magnitude smaller than the characteristic time of thermals. The temperature measurement is repeatable to $\pm 0.1°C$.

3. HEAT TRANSFER MEASUREMENTS

In the four configurations tested, HHCC, HHHC, HCCC and HC, the bottom of the enclosure is always heated. Since the flow in the cube is essentially a boundary layer driven by the temperature difference between a boundary surface and the core, the wall-to-bulk temperature difference is the temperature difference used to calculate the heat transfer coefficient, and thus the Nusselt number, for each wall. Therefore, the coefficient of the Rayleigh number in the Nusselt–Rayleigh correlations presented here is twice what it would be if the overall temperature difference had been used to calculate the heat transfer coefficient. This method of computing the Nusselt number is used here to collapse the hot- and cold-wall Nusselt numbers when the surface areas of the hot and cold walls are different. Note that, because of the simultaneous heating and cooling of the bottom, top and side surfaces, and subsequent interaction between the horizontal and vertical modes of heat transfer, it is not possible to determine how much energy transferred from a given heated surface is transferred to a given cooled wall. For the heat transfer experiments, note that $h = l$, the cold surfaces are all the same temperature, typically 15°C, and that the hot surfaces are all the same temperature, typically 45°C. We will also drop the l and h subscripts for this section.

The HHCC configuration involves simultaneous heat transfer from the bottom surface and a vertical side

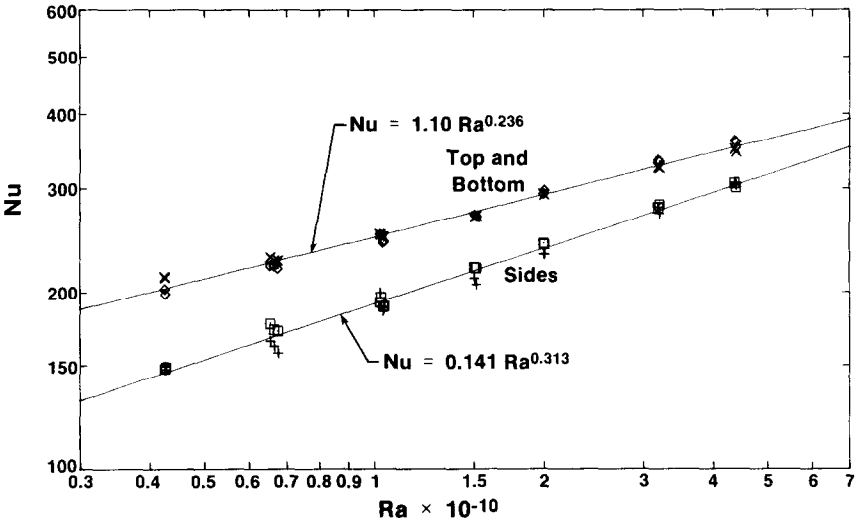

FIG. 3. Heat transfer data and correlations for the HHCC configuration.

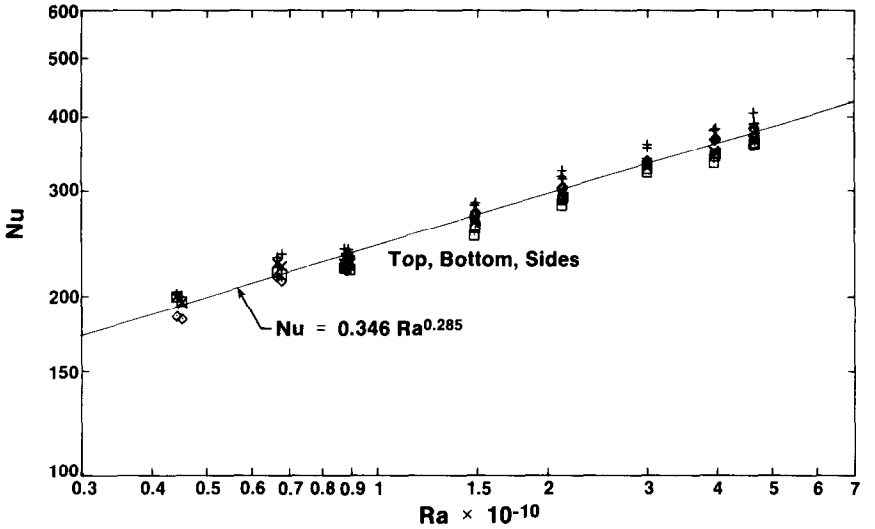

FIG. 4. Heat transfer data and correlations for the HCCC configuration.

wall to the top surface and the opposite vertical side wall. The data points and corresponding correlation equations are plotted in Fig. 3. The Nusselt numbers for the bottom and top surfaces are almost identical, and are given by

$$Nu = 1.10Ra^{0.236}. \quad (3)$$

The Nusselt numbers for the walls are best correlated by

$$Nu = 0.141Ra^{0.313}. \quad (4)$$

The bottom- and top-surface Nusselt numbers are about 25% higher than the side-wall Nusselt numbers. Therefore, the dominant mode of heat transfer in this Rayleigh-number range is turbulent natural convection from the bottom to the top of the enclosure rather than laminar boundary-layer heat transfer from one vertical wall to another. The interaction of the two types of heat transfer has an effect on the exponent of the Rayleigh number. The Rayleigh number exponent for the top and bottom surfaces is lower than that predicted by equation (1), and the Rayleigh number exponent for the walls is higher than that predicted by equation (2).

In the HCCC configuration, heat is transferred from the bottom of the enclosure to both walls and to the ceiling. In this case, there is no heat transfer from one vertical wall to another. As shown in Fig. 4, the Nusselt numbers for all four walls collapse to a single correlation:

$$Nu = 0.346Ra^{0.285}. \quad (5)$$

The heat transfer to both walls and to the top was the

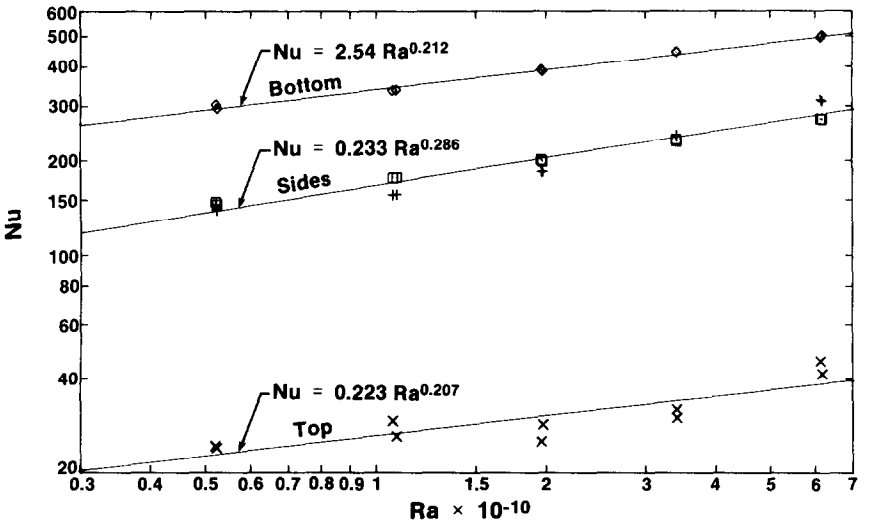

FIG. 5. Heat transfer data and correlations for the HHHC configuration.

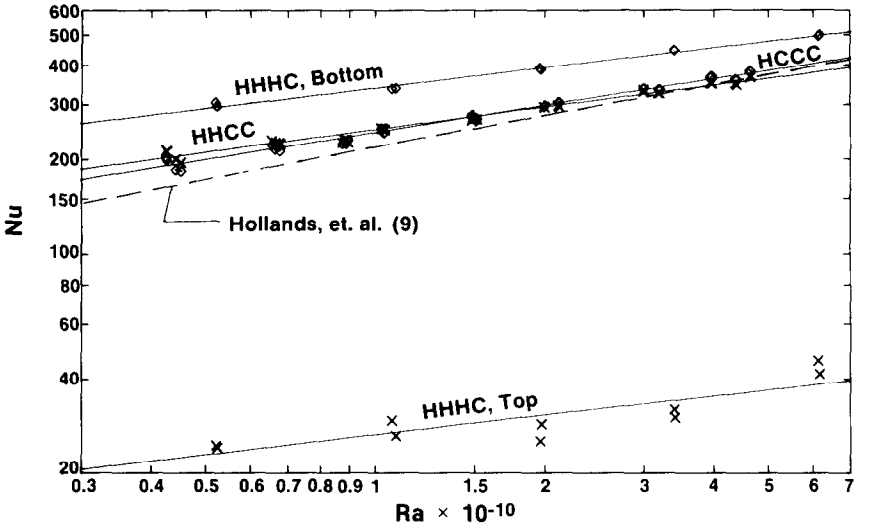

FIG. 6. Comparison of heat transfer data for top and bottom surfaces of configurations HHCC, HHHC and HCCC, and a correlation for top and bottom heating/cooling.

same, which is an unanticipated result. The exponent of the Rayleigh number is very close to previous experimentally measured exponents for the vertical configuration.

The HHHC configuration is one in which heat is transferred from the top, the bottom, and one vertical wall to the opposite vertical wall. The results for this configuration are plotted in Fig. 5. The heat transfer and Nusselt numbers for the bottom surface are about an order of magnitude larger than those for the top surface. The dominant mode of heat transfer is convection from the heated bottom surface to the cooler wall. The Nusselt number correlation from the bottom surface is

$$Nu = 2.54Ra^{0.212}. \quad (6)$$

The vertical, i.e. the bottom- and top-surface, Nusselt numbers for the last three configurations are compared to the predictions of equation (1) in Fig. 6. The configuration HHHC exhibited the largest bottom-surface Nusselt number and the smallest top-surface Nusselt number. The results for the HHCC and HCCC configurations were very close to equation (1). This indicates that the thermal boundary conditions of the side walls do not greatly affect the heat transfer from the bottom surface to the top surface for Rayleigh numbers

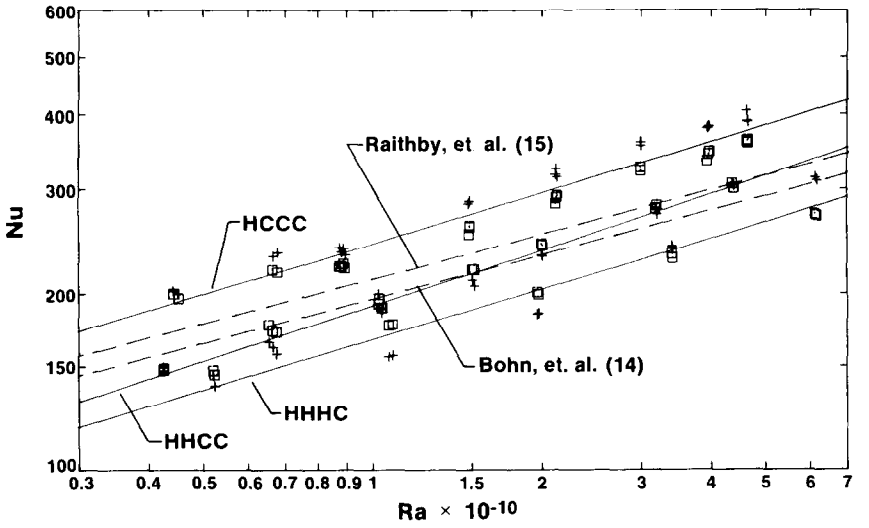

FIG. 7. Comparison of heat transfer data for side walls for the configurations HHCC, HHHC and HCCC, and two correlations for side-wall heating/cooling only.

near 10^{10}. Changing the top-surface boundary condition from cold to hot, as in the HHCC and HHHC configurations, increases the bottom-surface Nusselt number by about 40% and decreases the top-surface Nusselt number by about an order of magnitude.

The horizontal wall Nusselt number correlations from the last three configurations are compared with equation (2) in Fig. 7. We have also plotted a correlation of previous results from the same experimental apparatus involving the limiting case of heated and cooled side and end walls and adiabatic top and bottom surfaces, as reported by Bohn *et al.* [14]. The largest wall Nusselt numbers, about 20% higher than the limiting cases, occurred in the HCCC configuration.

The *Nu–Ra* data points for the HHCC configuration have a steeper slope than the limiting case, and intersect the limiting case in the middle of the Rayleigh number range. The wall Nusselt numbers for the HHHC configuration are about 20% lower than the limiting case.

Changing the top-surface boundary condition from cold to hot while maintaining differentially heated side walls decreases the wall Nusselt numbers by about 20%. In the HHCC configuration, it is possible to transfer heat from the hot wall to the cold top, while it is not possible in the HHHC configuration. The boundary layer on the hot wall in the HHHC configuration must traverse along the hot top surface before transferring heat to the opposite cold wall. In the HCCC configuration, the cold-wall boundary layers can exchange heat directly with the hot floor, which produces relatively higher heat transfer.

The limiting configuration HC was tested with a constant heat flux bottom surface produced by electrical resistance heating. Temperature measurements on the test cell floor at 16 equally spaced locations indicate a spatial temperature variation of approx. 0.9°C or 3% of the overall temperature difference and therefore the bottom surface may be considered essentially isothermal. Heat transfer data are shown in Fig. 8 in the form of Nu vs Ra^* and are compared with Holland's conduction-layer model, equation (1). The comparison is quite good although the present data appear to be shifted down by about 3%. The data are correlated well by

$$Nu = 0.176 Ra^{*1/4}, \tag{7}$$

which is equivalent to a 1/3 power dependence of Ra.

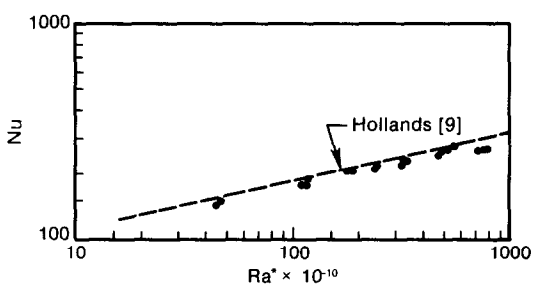

FIG. 8. Heat transfer data and correlations for the HC configuration.

4. FLOW PATTERNS

A typical shadowgraph of the limiting HC case is shown in Fig. 9. The gridlines in the photograph are spaced at distances equal to 5% of the test cell dimension, i.e. 1.52 cm. Thermals rising from the floor and falling from the ceiling are evident. The thermals are of varying characteristic sizes, averaging about 10 mm in height and 5 mm in width. There is no overall flow pattern discernable, other than the mixing motion of the thermals. The thermals appeared to be released periodically from the top of a boundary layer about 1 mm away from the surface and propagate at about 5 cm s^{-1}. Only the larger thermals were able to penetrate to the opposite side of the cavity. The thermals usually moved at some random angle (less than 45°) to the vertical.

A shadowgraph of the HHCC case in which the side walls are differentially heated is shown in Fig. 10. Relative to the figure, the left side wall is heated, and the right side wall is cooled. The interaction of the thermals and the boundary layers is clearly evident. In this case, the thermals are shifted by the side-wall boundary layers into triangular regions in the upper right and lower left corners of the cavity. A close up of the upper right of the HHCC case is shown in Fig. 11. The overall flow pattern is one of counterclockwise motion along the perimeter of the enclosure. The main effect of the boundary layer is convection of the thermals in a counterclockwise direction. The thermals in turn cause the boundary layer to separate at some point along the horizontal traverse. It is interesting to note that the vertical and horizontal Nusselt numbers for this configuration are very close to their limiting cases, indicating that the interactions visible in Figs. 10 and 11 have a small effect on the overall heat transfer from each surface.

A shadowgraph of the HCCC configuration with both side walls cooled is shown in Fig. 12. The overall flow pattern is similar to that predicted in Chan and Banerjee [1], with a central rising plume of thermals which diverges at the top of the cavity and returns along the cold side walls. The shadowgraph is focused on the central floor area where the rising plume originates. The plume is not centered, and its location was found to be very sensitive to changes in the initial conditions of the experiment. Thus, the rising thermals are located near the center of the tank, and the falling thermals are located near the cold side walls. Such a flow pattern is essentially a mixed free and forced convection situation for the side walls, which would explain why the Nusselt numbers for this case (given in ref. [5]) are higher than the other cases. The increase in side-wall heat transfer is enough to make it approximately equal to the vertical heat transfer.

A shadowgraph of the HHHC configuration, with a heated top and differentially heated side walls, revealed very little activity in the core of the cavity, especially near the ceiling. The motion of the thermals was confined to within 10 mm of the heated bottom plate.

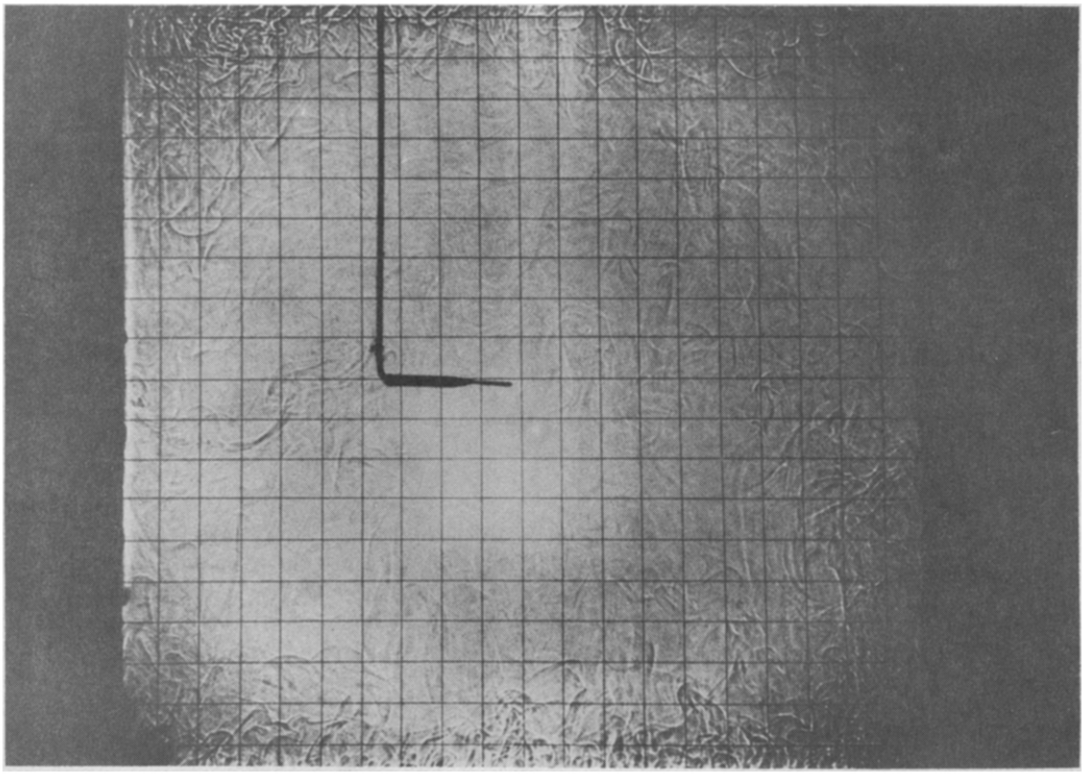

FIG. 9. Shadowgraph of HC flow patterns.

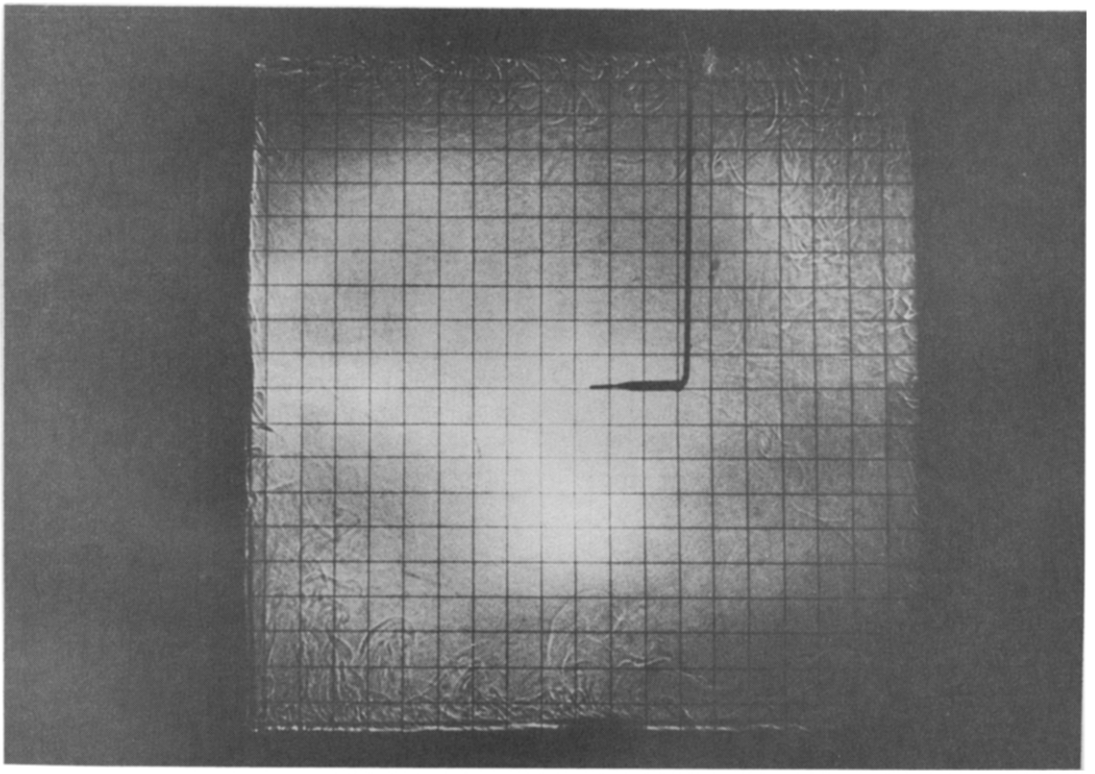

FIG. 10. Shadowgraph of HHCC flow patterns.

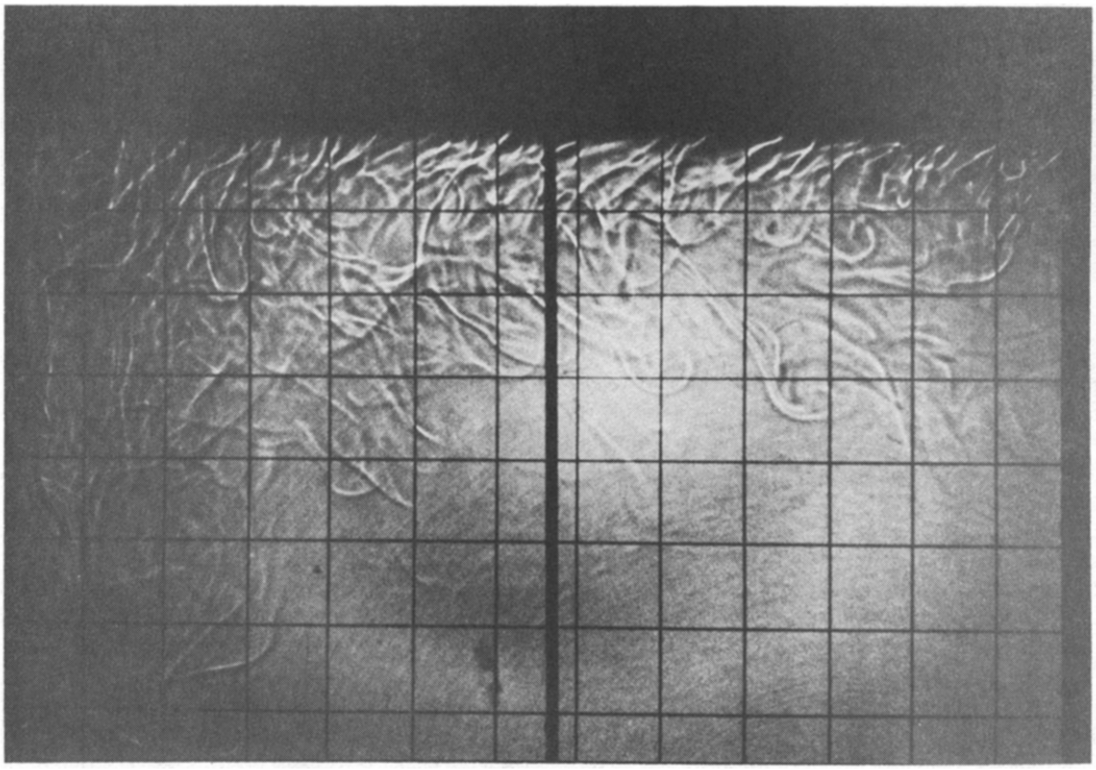

FIG. 11. Shadowgraph of HHCC flow patterns in upper right corner.

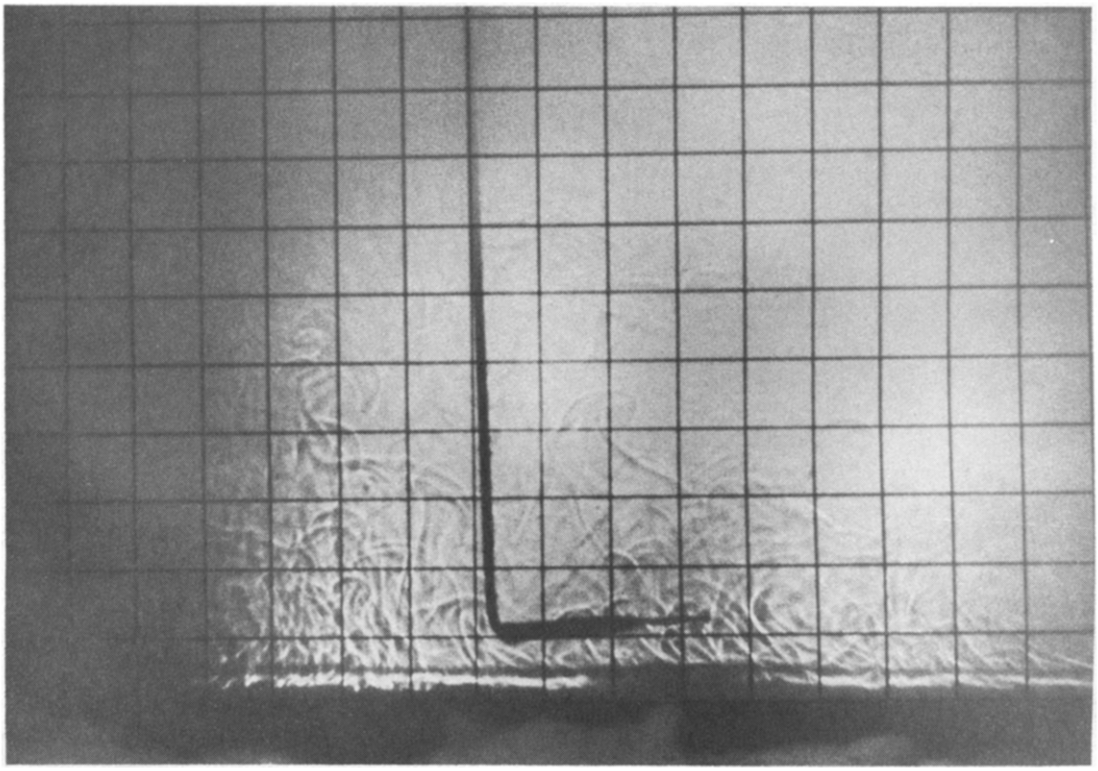

FIG. 12. Shadowgraph of HCCC flow patterns.

Boundary layers were observed on the side walls, but not along the top surface. Temperature measurements (to be discussed in the next section) revealed stable stratification in the core due to the heated top. The low Nusselt number of the ceiling as shown in Fig. 5 is due to the stable stratification in the core. The relatively low side-wall Nusselt numbers as shown in Fig. 8 are due to the weakening of side-wall boundary layers by the stratification induced by the heated top.

5. TEMPERATURE DISTRIBUTION

The thermals seen in the shadowgraphs affect the temperature distribution in the test cell. To record temperature disturbances induced by the thermals, the thermocouple probe was placed as near as possible (8 mm) to the bottom and top surfaces of the test cell. A time series record of the thermocouple output is shown in Fig. 13. Thermals rising from the bottom of the test cell and falling from the top of the test cell are evident. For the HC configuration shown the thermals disturb the fluid from a baseline temperature. For the other configurations, the disturbance is somewhat more irregular. The magnitude of the temperature disturbance is of the order of 1°C. The period is of the order of 4 s.

The mean temperature distribution in the vertical midplane of the test cell is shown in Fig. 14. The temperature is plotted relative to the bulk temperature, defined earlier. These results generally support the use of the bulk temperature in the heat transfer correlations. For the HC, HHCC, and HCCC configurations the core of the fluid is within 0.5°C of the bulk temperature. For the HHHC configuration which has a heated ceiling, the core of the fluid is within 4°C of the bulk temperature. The results of this configuration show that a nonzero Ra_h, i.e. a finite temperature difference between the top and bottom of the enclosure, is required to produce a destratified core. The heated top in the HHHC configuration prevents heat transfer out of the top of the enclosures as is the case for the other three configurations. Heat transfer out of the enclosure is possible only through the cold side wall as in the limiting case of differential side heating with an adiabatic top and bottom. Fluid particles that are heated by the hot floor or hot side wall and rise to the top of the enclosure will then maintain temperatures warmer than the bulk temperature. Fluid particles that are cooled by the side wall will sink near the floor and be cooler than the bulk temperature. In fact, as the probe was moved horizontally toward the cooled wall, the mean fluid temperature at $z/h = 0.025$, the lowest probe location, went from 3° to 7° cooler than the bulk temperature. In this case the thermals do not act as a mixing mechanism for the core. They act as the mechanism for local heat transfer from the floor. The HC and HHCC profiles show a slight temperature reversal, near the top and bottom surfaces, due to the persistence of the thermals traversing across the enclosure.

In order to investigate the influence of different vertical Rayleigh numbers, Ra_h, on the core tempera-

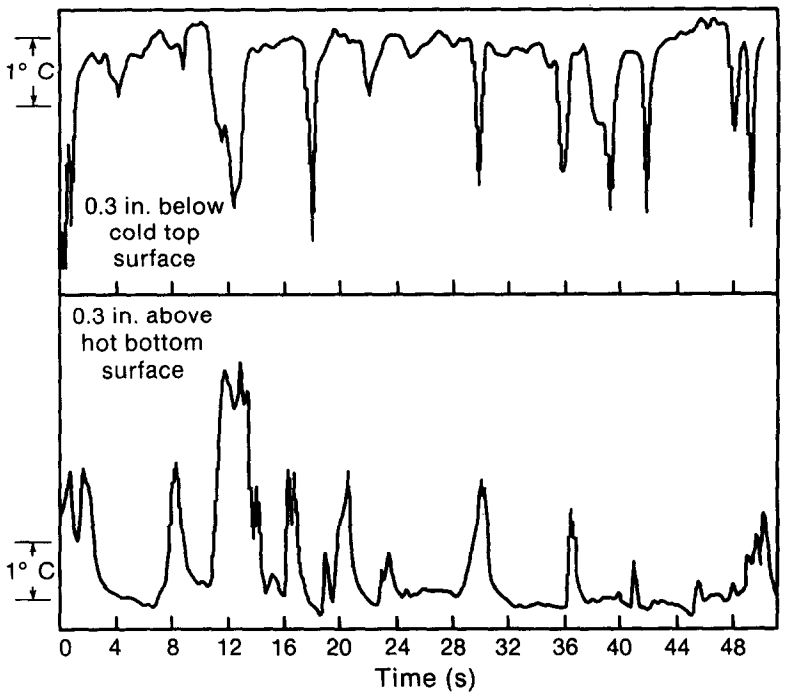

FIG. 13. Temperature record for HC configurations.

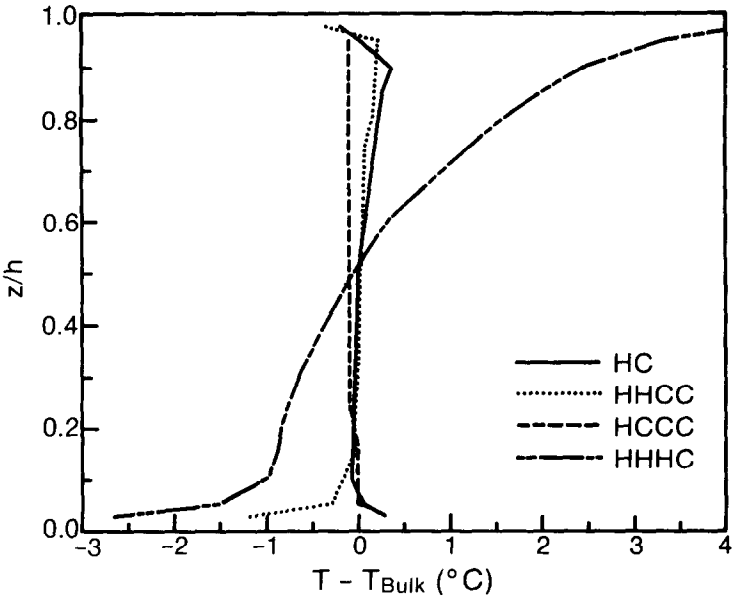

FIG. 14. Mean temperature profiles ($Ra = 1.45 \times 10^{10}$).

ture distribution, the temperature of the heated floor in the HHCC configuration was varied from 20.8° to 39.8°C, while the heated wall was kept near 39°C, and the cooled top and side were kept near 17°C. The vertical Rayleigh number, Ra_h, thus varied from 0.1×10^{10} to 1.45×10^{10}, while the horizontal Rayleigh number, Ra_l, varied slightly from 1.14×10^{10} to 1.45×10^{10}.

The resulting core temperatures in the center of the enclosure are shown in Fig. 15. The data show that as the vertical Rayleigh number is increased, the level of stratification in the core of the fluid is decreased. The change in stratification is not gradual, but rather sudden at a Ra_h of about 0.65×10^{10}. Also, the stratification is not symmetric about $z/h = 0.5$, due to the nonsymmetric top and bottom temperature boundary conditions. As the temperature of the floor is increased, the temperature difference between the floor and the core increases, which eventually results in the formation of thermals vigorous enough to cause mixing of the core.

The nondimensional temperature fluctuations for the vertical midplane of each of the four configurations are shown in Fig. 16. The fluctuations are computed by dividing the standard deviation of the temperature, σ, by the hot–cold wall temperature difference, which was

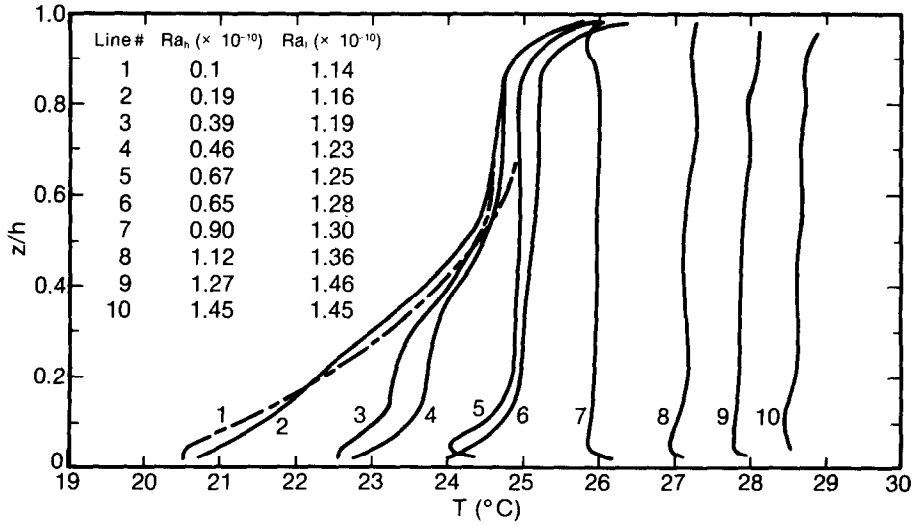

FIG. 15. Mean temperature profiles for varying Ra_h in HHCC configuration.

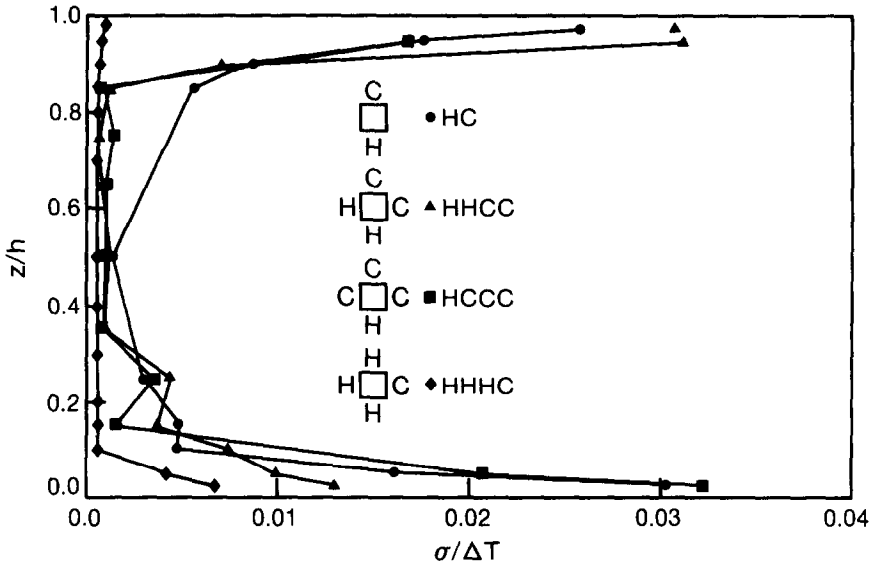

FIG. 16. Temperature fluctuation profiles ($Ra = 1.45 \times 10^{10}$).

typically 25°C. The largest fluctuations of about 0.03 were measured nearest the floor and ceiling, and the smallest values of about 0.001 were measured in the middle of the test cell. With the exception of the upper 15% of the HHHC configuration the curves are very similar. The temperature fluctuation near the ceiling of the HHHC configuration remains at the 0.001 level of the core due to the stable stratification induced by the heated ceiling. A very slight increase can be noted near the ceiling, due to the boundary layer from the heated vertical wall. It is difficult to compare the fluctuation levels with previously published results such as [6] and [7] since the temperature probe could not be placed closer than 8 mm to a horizontal surface.

Additional nondimensional temperature fluctuation for the HHCC configuration with $Ra_h = Ra_l$ are presented in Fig. 17. Lines of constant nondimensional temperature fluctuation are plotted for the half of the enclosure near the cold vertical wall. The contours near the cold top show that the descending thermals are being swept toward the cold wall by the rotation induced by the differentially heated side walls as also seen in Fig. 10. The largest fluctuations are at the corner of the cold side wall and the hot floor, due to the impingement of the cold-wall boundary layer on the hot floor. The fluctuations at the vertical midline are much smaller than the fluctuations nearer the edges of the enclosure.

6. SUMMARY AND CONCLUSIONS

This paper presents results of an experimental investigation of the mixed cavity problem at high Rayleigh number. In particular, differentially heated and cooled vertical and horizontal surfaces have been tested in four configurations in order to elucidate the interaction of thermals released from the horizontal surfaces with the boundary layers on the vertical surfaces. Generally, the heated floor promotes mixing in the cavity and tends to eliminate the stratification seen in the limiting case of a horizontal temperature

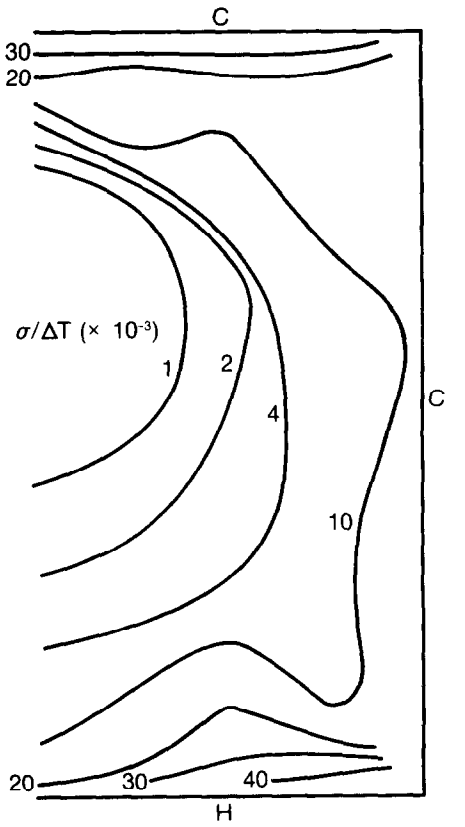

FIG. 17. Lines of constant temperature fluctuation for HHCC configuration with $Ra_h = Ra_l = 1.45 \times 10^{10}$.

difference alone. Although the temperature disturbances associated with the thermals appear to persist for only a small distance from the horizontal surfaces, the thermals are effective in mixing the core fluid. For the limiting case of an unstable vertical temperature difference alone, the only motion in the test cell is that of the thermals. In this case, the heat transfer from the heated floor compares favorably to a conduction-layer model.

The addition of a horizontal temperature difference to this limiting case imparts a rotation to the core fluid and a horizontal velocity component to the thermals. For this configuration the heat transfer from the horizontal surfaces is not strongly affected by the addition of a horizontal temperature difference, however, the thermals do affect the heat transfer from the vertical surfaces. Heat transfer from the vertical surfaces is reduced if the cavity top is heated. This is due to the stable stratification in the top portion of the cavity core.

Acknowledgements—The first author was supported by the Faculty Research Program of the American Society for Engineering Education. This support is gratefully acknowledged.

REFERENCES

1. A. M. C. Chan and S. Banerjee, A numerical study of three dimensional roll cells within rigid boundaries. *J. Heat Transfer* **101,** 233–237 (1979).
2. G. S. Shiralkar and C. L. Tien, A numerical study of the effect of a vertical temperature difference imposed on a horizontal enclosure, *Num. Heat Transfer* **5,** 185–197 (1982).
3. I. Catton, Natural convection in enclosures, *Proc. 6th Int. Heat Transfer Conference*, Toronto, Canada, Vol. 6, pp. 13–31 (1978).
4. S. Ostrach and C. Raghavan, Effect of stabilizing thermal gradients on natural convection in rectangular enclosures, *J. Heat Transfer* **101,** 238–243 (1979).
5. B. M. Berkovsky, V. E. Fertman, E. F. Nogotov, E. A. Lipkina and V. G. Bashtovi, Free convection, *Prog. Heat Mass Transfer* **9,** 191–233 (1971).
6. E. F. Somerscales and I. W. Gazda, Thermal convection in high Prandtl number liquids at high Rayleigh numbers, *Int. J. Heat Mass Transfer* **12,** 1491–1511 (1969).
7. T. Y. Chu and R. J. Goldstein, Turbulent convection in a horizontal layer of water, *J. Fluid Mech.* **60,** 141–159 (1973).
8. A. M. Garon and R. J. Goldstein, Velocity and heat transfer measurements in thermal convection, *Phys. Fluids* **16,** 1818–1825 (1973).
9. K. G. T. Hollands, G. D. Raithby and L. Konicek, Correlation equations for free convection heat transfer in horizontal layers of air and water, *Int. J. Heat Mass Transfer* **18,** 879–884 (1975).
10. T. Fujii and H. Imura, Natural convection heat transfer from a plate with arbitrary inclination, *Int. J. Heat Mass Transfer* **15,** 755–767 (1972).
11. L. N. Howard, Convection at high Rayleigh number, *Proc. 11th Int. Congress of Applied Mechanics*. Springer, Berlin, pp. 1109–1115 (1964).
12. E. M. Sparrow, R. B. Husar and R. J. Goldstein, Observations and other characteristics of thermals, *J. Fluid Mech.* **41,** 793–800 (1970).
13. R. K. MacGregor and A. F. Emery, Free convection through vertical plane layers—moderate and high Prandtl number fluids, *J. Heat Transfer* **91,** 391–403 (1969).
14. M. S. Bohn, A. T. Kirkpatrick and D. A. Olson, Experimental study of three-dimensional natural convection at high Rayleigh number, *J. Heat Transfer* **106,** 339–345 (1984).
15. G. D. Raithby, K. G. T. Hollands and T. E. Unny, Analysis of heat transfer by natural convection across vertical fluid layers, *J. Heat Transfer* **99,** 287–293 (1977).

RECHERCHE EXPERIMENTALE SUR LA CONVECTION NATURELLE EN CAVITE, AUX REGIMES DE NOMBRE DE RAYLEIGH ELEVE

Résumé—On réalise des expériences de convection naturelle aux nombres de Rayleigh élevés, dans une cavité cubique avec quatre conditions différentes de chauffage ou de refroidissement sur les surfaces verticales ou horizontales. Les mesures et les observations portent sur le transfert thermique, les configurations d'écoulement et les distributions moyenne et fluctuante de température. Les résultats montrent que le plancher chauffé favorise le mélange dans la cavité et réduit la stratification thermique. Pour les conditions aux limites expérimentées, le transfert thermique aux surfaces horizontales n'est pas fortement influencé par la présence d'un gradient de température horizontal.

EINE EXPERIMENTELLE UNTERSUCHUNG DER NATÜRLICHEN KONVEKTION IN EINEM HOHLRAUM BEI HOHEN RAYLEIGHZAHLEN

Zusammenfassung—An vier verschiedenen Anordnungen von abwechselnd beheizten und gekühlten senkrechten und waagerechten Flächen in einem würfelförmigen Hohlraum wurden Untersuchungen der natürlichen Konvektion bei hohen Rayleighzahlen durchgeführt. Alle Versuche waren Variationen des Falles mit Beheizung von unten. Messungen und Beobachtungen des Wärmeüberganges, der Strömungsformen sowie des Mittelwertes und der Schwankungen der Temperatur wurden durchgeführt. Die Ergebnisse zeigen, daß die Beheizung des Bodens eine Durchmischung im Hohlraum verursacht und die thermische Schichtung abbaut. Bei den vorhandenen Randbedingungen wurde der Wärmeübergang an den waagerechten Flächen nicht wesentlich von der Existenz eines Temperaturgradienten beeinflußt.

ЭКСПЕРИМЕНТАЛЬНОЕ ИССЛЕДОВАНИЕ СМЕШАННОЙ ЕСТЕСТВЕННОЙ КОНВЕКЦИИ В ПОЛОСТИ ПРИ БОЛЬШИХ ЗНАЧЕНИЯХ ЧИСЛА РЭЛЕЯ

Аннотация—Проведено экспериментальное исследование четырех различных по форме и поразному нагреваемых и охлаждаемых вертикальных и горизонтальных поверхностей кубической полости при больших значениях числа Рэлея. Во всех экспериментах изменялась величина теплового потока при нагреве снизу. Исследованы и измерены тепловой поток, режим течения и распределения средней пульсационной температуры. Результаты показывают, что нагрев снизу ведет к перемешиванию в полости и уменьшает тепловую стратификацию. При граничных условиях, реализованных в эксперименте, теплоперенос от горизонтальных поверхностей слабо зависит от горизонтального градиента температур.